Ultrathin silicon-on-insulator vertical tunneling transistor

A. Zaslavsky[a)] and C. Aydin
Division of Engineering and Department of Physics, Brown University, Providence, Rhode Island 02912

S. Luryi
Department of Electrical Engineering, SUNY−Stony Brook, Stony Brook, New York 11794

S. Cristoloveanu
IMEP-ENSERG, 23 rue des Martyrs, Grenoble, France

D. Mariolle, D. Fraboulet, and S. Deleonibus
CEA-DRT, LETI/DTS, CEA, 17 rue des Martyrs, Grenoble, France

We have fabricated silicon-on-insulator (SOI) transistors with an ultrathin Si channel of ∼5 nm, tunneling gate oxide of ∼1 nm, and 100 nm gate length. In addition to good transistor characteristics, these same devices exhibit additional functionality at low temperature. The drain current I_D exhibits steps near the turn-on threshold voltage as a function of the backgate V_{BG} bias on the substrate. When operated as a gate-controlled tunneling device, with source shorted to drain and I_G originating from tunneling from the gate to the channel, we observe structure in the $I_G(V_{BG})$ due to resonant tunneling into the quantized channel subbands. In the future, as SOI device fabrication improves and the buried oxide thickness is reduced, these quantum effects will become stronger and appear at lower V_{BG}, offering the prospect of ultralarge scale integration-compatible devices with standard transistor operation or quantum functionality depending on the electrode biasing. © *2003 American Institute of Physics.* [DOI: 10.1063/1.1600832]

Silicon-on-insulator (SOI) transistors built in thin fully depleted Si channels on top of an insulating buried oxide are predicted by the various technology roadmaps[1] to take over from bulk Si complementary metal–oxide–semiconductor (CMOS) devices over the next few years, leading to an ongoing debate about an appropriate double-gate SOI transistor architecture.[2] At the same time, the ongoing miniaturization of SOI devices, with available Si channel and gate insulator thicknesses dropping to the nanoscale, is opening the door to quantum effect devices based on tunneling and/or charge quantization fabricated in and integrable with mainstream CMOS. This is significant because it appears increasingly unlikely that any incompatible quantum effect architecture will make inroads against the rapidly evolving CMOS technology.[3] To date, most of the work in CMOS-compatible tunneling transistors has focused on quantum dots replacing the usual channel,[4–6] wherein the tunneling into discrete levels combined with Coulomb charging produces a sharply peaked $I_D(V_G)$ characteristic. Here we report on a device, produced by a conventional technological process, that combines standard $I_D(V_G)$ curves under ordinary transistor biasing and a backgate controlled tunneling current $I_G(V_{BG})$ when operated in the quantum capacitance mode.[7]

One of the most widely studied quantum effect devices is the resonant tunneling (RT) structure, where strongly nonlinear current–voltage $I(V)$ characteristics and negative differential resistance (NDR) arise due to carrier tunneling selection rules into a reduced dimensionality density of states [a quantum well (QW) or dot confined by tunneling barriers].[8,9] The difficulty with Si-based RT structures has been the absence of sufficiently high heteroepitaxial barriers. Technologically compatible strained Si/SiGe pseudomorphic

RT structures[10,11] operate with tunneling barriers in the 0.2–0.3 eV range, leading to low-temperature operation and much less pronounced NDR—suitable for spectroscopy of confined states in SiGe QWs and dots,[12,13] but problematic for devices. Other Si-based resonant tunneling structures involve exotic materials, such as CaF_2.[14] In this letter, we report on a tunneling structure with SiO_2 barriers built in the standard SOI transistor geometry with $L_G=0.1$ μm gate length, shown in Fig. 1(a). The key difference is that the Si channel is thinned down to ∼5 nm, to foster quantization in the channel, and the gate oxide is reduced to ∼1 nm to create a tunneling barrier. Despite these stringent criteria, these devices exhibit good transistor $I_D(V_G)$ and $I_D(V_{BG})$ curves at both room and cryogenic temperatures [V_{BG} refers to biasing the substrate under the buried oxide, see Fig. 1(a)]. At low temperature we observe two quantum effects. First, the drain current $I_D(V_{BG})$ at small V_D exhibits clear steps near the threshold, corresponding to channel subbands becoming available for charge transport, indicating sufficient uniformity of the Si channel over the entire active region under the gate. Second, when the device is operated in a purely tunneling mode—source shorted to drain, with drain current due only to tunneling from the gate—we observe structure in the $I_D(V_{BG})$ due to the changing alignment of the quantized channel subbands with the occupied states in the gate, as predicted by the quantum capacitance mechanism[7] and first observed in III–V structures.[15]

The devices were fabricated on an 8 in. silicon line at LETI-CEA on standard UNIBOND SOI substrates (400 nm of buried oxide) using an existing CMOS mask set. The active region Si was thinned to 50 nm using repeated sacrificial oxidation and removal and then locally thinned to ∼5 nm in the gate region.[16] The thermal gate oxide was kept as thin as possible by densifying the native oxide, resulting in ∼1 nm

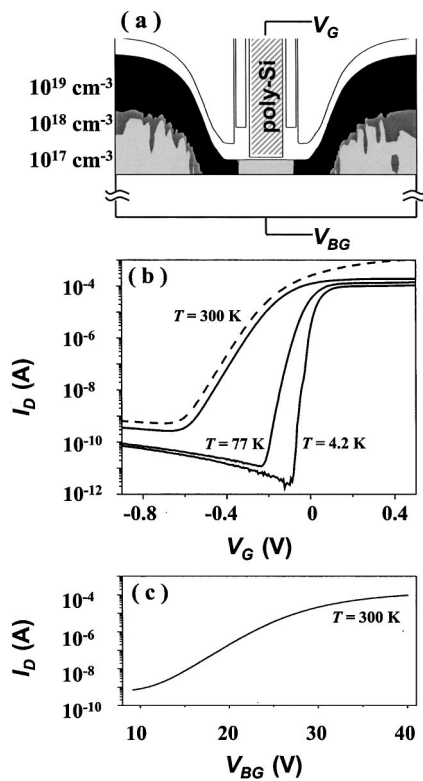[a)]Electronic mail: alexander_zaslavsky@brown.edu

FIG. 1. (a) Cross-sectional view of the device: the Si channel thickness under the gate is ~ 5 nm thick, the front gate oxide is ~ 1 nm. Grayscale contours show the 10^{19}, 10^{18}, and 10^{17} cm^{-3} doping contours in the source and drain extensions, the channel under the gate is essentially undoped. (b) Standard $I_D(V_G)$ transfer characteristics at $T=300$, 77, and 4.2 K for $V_D=0.1$ V (and 0.6 V at $T=300$ K, dashed line), $V_{BG}=0$. (c) Backgate $I_D(V_{BG})$ transistor characteristics for $V_D=0.1$ V, $V_G=-0.8$ V at $T=300$ K.

SiO$_2$. After *in situ* doped poly-Si gate material (P-doped to $\sim 10^{19}$ cm^{-3} range), the device followed standard transistor processing with low-energy (3 keV) As source/drain implants. The dimensions of the transistors reported here were gate length $L_G=0.1$ μm and width of 10 μm. The fabrication sequence was simulated on Silvaco software, using the actual implantation and activation anneal parameters. The resulting cross-sectional view of the device is illustrated in Fig. 1(a).

Standard transistor $I_D(V_G, V_{BG}=0)$ characteristics for $V_D=0.1$ V are shown in Fig. 1(b) for $T=300$, 77, and 4.2 K. Because of n^+-poly gate material, the threshold $V_T<0$, but otherwise the room-temperature characteristics show good subthreshold slope and acceptable drain-induced barrier lowering (compare $V_D=0.1$, 0.6 V at $T=300$ K). Detailed performance analysis of these devices as standard transistors will be published elsewhere.[17] Once the channel is depleted with $V_G<V_T$, an even more negative V_G results in a slowly increasing and relatively temperature-insensitive tunneling current through the ultrathin gate oxide. Given the SOI geometry, the transistor can also be turned on using the substrate backgate voltage V_{BG}. Figure 1(c) shows the room-temperature $I_D(V_{BG}, V_G=-0.8$ V) curve at $V_D=0.1$ V.

At $T=4.2$ K, below the threshold $V_G \lesssim -0.1$ V and at small $V_D=1$ mV, I_D exhibits clear current steps as the transistor is turned on by V_{BG}, as shown in Fig. 2. These steps, which persist in a weaker fashion to $T=77$ K, correspond to quantized subbands in the Si channel being pulled down below the source Fermi level. As is clear from Fig. 2, changing front-gate V_G shifts the $I_D(V_{BG})$ curve along the V_{BG} axis:
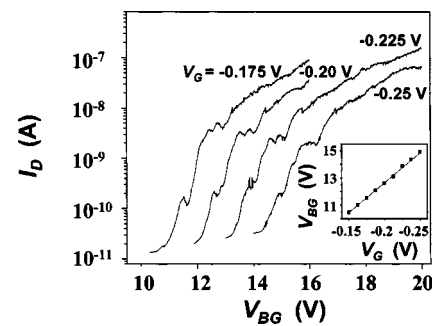

FIG. 2. Drain current $I_D(V_{BG})$ characteristic at $T=4.2$ K and $V_D=1$ mV for several values of $V_G<V_T$. The current steps correspond to the population of quantized subbands E_n in the channel under the gate. Inset of Fig. 2 plots the V_{BG} position of the first current step vs V_G.

for $\Delta V_G=12.5$ mV, the corresponding $\Delta V_{BG} \sim 0.6$ V due to ratio of the buried oxide thickness to the combination of top oxide and Si channel thicknesses—see inset of Fig. 2. The results of Fig. 2 are quite similar to the Si quantum dot transistors,[4–6] except that in dots the I_D exhibits sharp peaks followed by NDR regions corresponding to tunneling into discrete states, whereas here we have tunneling into effectively two-dimensional (2D) subbands E_n in the channel. Since these 2D subbands contain higher-energy states corresponding to in-plane motion, the NDR is weakened by impurity and phonon scattering-assisted tunneling into these states.[18] Also, inhomogeneities in the Si channel thickness and the SiO$_2$/Si interface are certain to broaden E_n and, hence, the $I_D(V_{BG})$ steps.

Figure 3 illustrates the quantum capacitance mode of operation of this device. The gate is grounded and acts as the
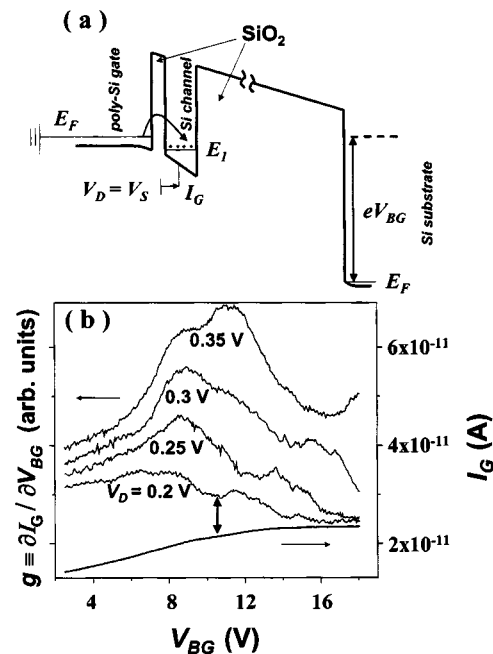

FIG. 3. (a) Schematic vertical band diagram through the device midpoint under bias, indicating the electron tunneling into the quantized Si channel (only the lowest subband E_1 is shown) and their subsequent lateral extraction via the (shorted) source and drain contacts. Control of the tunneling current I_G via V_{BG} is due to the penetration of the electric field through the Si channel, which alters the alignment of E_1 with poly-Si gate E_F. (b) Tunneling $I_G(V_{BG})$ characteristic at $T=4.2$ K for $V_S=V_D=0.2$ V (arrow marks the transconductance $g \equiv \partial I_G / \partial V_{BG}$ minimum), together with smoothed $g(V_{BG})$ for various $V_S=V_D=0.2$–0.35 V.

"emitter," the source and drain electrodes are shorted and biased to a V_D, and I_G is modulated by the substrate voltage V_{BG}.[7] The schematic vertical band diagram through the midpoint of the device and the tunneling current is shown in Fig. 3(a), with the ~1 nm gate oxide acting as the thin first barrier, the buried oxide acting as an impenetrable second barrier, and the thinned Si channel acting as the QW containing 2D subbands E_n (only E_1 is shown). Electrons tunnel from the n^+-poly-Si gate into E_1 and are extracted laterally via the source and drain contacts. The tunneling I_G is the only current component in this biasing mode (no measurable substrate leakage is observed for any V_{BG}). As in all RT structures, this tunneling I_G depends on the alignment of E_1 with the occupied states in the gate—see Fig. 3(a). Three-terminal operation is achieved via V_{BG}, which induces an electric field and alters the alignment between the channel and the gate.[7,9] In principle, once E_1 is lowered below the bottom of the occupied states in the gate electrode, I_G is cut off by the energy and transverse momentum conservation.[8] This should lead to a negative transconductance, $g \equiv \partial I_G/\partial V_{BG} < 0$, but the effect is weakened by energy or transverse momentum nonconserving tunneling, as well as broadening of E_1 due to Si channel nonuniformity and the possible inhomogeneous broadening of the emitter states in the gate electrode due to quantum-size energy shifts in small poly-Si grains.[19]

The first observation of this phenomenon in a Si-based device is shown in Fig. 3(b), where we plot the $I_G(V_{BG})$ and the transconductance $\partial I_G/\partial V_{BG}$ for $V_G = 0$ and V_D ranging 0.2–0.35 V ($V_S = V_D$). As V_{BG} is increased from 0, the backgate transconductance $g \equiv \partial I_G/\partial V_{BG}$ for any given value of V_D first increases and then drops, with one or more (at higher V_D) clear minima in-between. The initial increase of g with V_{BG} corresponds to the V_{BG}-induced lowering of E_1 with respect to the gate, leading to a higher tunneling I_G. The eventual drop in g at large V_{BG} [that is, the near saturation of I_G as V_{BG} exceeds ~15 V at $V_D = 0.2$ V, see Fig. 3(b)], corresponds to a large carrier density being established in the Si channel. The tunneling oxide emitter barrier is then completely screened from the electric field produced by V_{BG}. The minima in g at intermediate V_{BG} corresponds to the E_1 subband going out of alignment with the occupied states in the gate. The actual alignment of the 2D subbands with the gate is a complex electrostatic problem that will be the subject of future study.

In estimating the potential impact of such devices, it is worth noting that an analogous RT structure was originally fabricated in a III–V heterostructure by Morkoç and co-workers.[15] There, both barriers were AlGaAs, with a much thicker second barrier ensuring the isolation between the GaAs QW and the substrate. The main technical difficulty in the III–V implementation was making good contact to the QW without leakage to the substrate. This problem is absent in SOI devices, where the buried oxide is essentially impenetrable. For the current generation of UNIBOND substrates, the required V_{BG} to shift quantized subbands in the Si channel runs to >10 V because of the 400-nm-thick buried oxide, but much thinner buried oxides will become available as SOI transistors are scaled down.

To summarize, we have fabricated proof-of-concept SOI resonant tunneling transistors, that combine standard transistor $I_D(V_G)$ transfer characteristics at large V_D with backgate control of the tunneling current $I_G(V_{BG})$ as the source and drain are shorted and the front gate is used as the emitter of the resulting RT structure. For now, the features in the tunneling transconductance are pronounced at $T = 4.2$ K, but with improved fabrication techniques the operating temperature will increase. As a result, our tunneling transistors offer, at least in principle, the prospect of enhancing silicon integrated circuits with SOI quantum tunneling devices featuring functionally useful nonlinear and NDR characteristics.

[1] The latest publicly released version of the ITRS roadmap is available on the http://public.itrs.net web site.

[2] G. K. Celler and S. Cristoloveanu, J. Appl. Phys. **93**, 4955 (2003).

[3] P. M. Solomon, in *Future Trends in Microelectronics: The Nano Millennium*, edited by S. Luryi, J. M. Xu, and A. Zaslavsky (Wiley-Interscience, New York, 2002), pp. 28–42.

[4] Y. Takahashi, M. Nagase, H. Namatsu, K. Kurihara, K. Iwadate, Y. Nakajima, S. Horiguchi, K. Murase, and M. Tabe, Electron. Lett. **31**, 136 (1995).

[5] E. Leobandung, L. Guo, Y. Wang, and S. Y. Chou, Appl. Phys. Lett. **67**, 938 (1995); E. Leobandung, L. Guo, and S. Y. Chou, *ibid.* **67**, 2338 (1995).

[6] M. Saitoh, T. Saito, T. Inukai, and T. Hiramoto, Appl. Phys. Lett. **79**, 2025 (2001).

[7] S. Luryi, Appl. Phys. Lett. **52**, 501 (1988).

[8] S. Luryi, Appl. Phys. Lett. **47**, 490 (1985).

[9] An overview of the quantum effect tunneling devices is available, for example, in S. Luryi and A. Zaslavsky, "Quantum effect and hot electron devices," chapter in *Modern Semiconductor Device Physics*, edited by S. M. Sze (Wiley-Interscience, New York, 1998), pp. 253–341.

[10] H. C. Liu, D. Landheer, M. Buchanan, and D. C. Houghton, Appl. Phys. Lett. **52**, 1809 (1988).

[11] Z. Matutinovic-Krstelj, C. W. Liu, X. Xiao, and J. C. Sturm, Appl. Phys. Lett. **62**, 603 (1993).

[12] U. Gennser, V. P. Kesan, D. A. Syphers, T. P. Smith III, S. S. Iyer, and E. S. Yang, Phys. Rev. Lett. **67**, 3828 (1991).

[13] J. Liu, A. Zaslavsky, and L. B. Freund, Phys. Rev. Lett. **89**, 096804 (2002).

[14] M. Watanabe, Y. Iketani, and M. Asada, Jpn. J. Appl. Phys., Part 2 **39**, L964 (2000); T. Terayama, H. Sekine, and K. Tsutsui, Jpn. J. Appl. Phys., Part 1 **41**, 2598 (2002).

[15] H. Morkoç, J. Chen, U. K. Reddy, T. Henderson, and S. Luryi, Appl. Phys. Lett. **49**, 70 (1986).

[16] D. Esseni, M. Mastrapasqua, G. K. Celler, F. H. Baumann, C. Fiegna, L. Selmi, and E. Sangiorgi, Tech. Dig. - Int. Electron Devices Meet. **2000**, 671 (2000).

[17] J. Prétet, A. Ohata, S. Cristoloveanu, C. Aydin, A. Zaslavsky, D. Mariolle, and S. Deleonibus (unpublished).

[18] V. J. Goldman, D. C. Tsui, and J. E. Cunningham, Phys. Rev. B **36**, 7635 (1987).

[19] N. Lifshitz, S. Luryi, and T. T. Sheng, Appl. Phys. Lett. **51**, 1824 (1987).